Investigation of Pt, Pt$_3$Co , and Pt$_3$Co / Mo Cathodes for the ORR in a Microfluidic H$_2$ / O$_2$ Fuel Cell

View the article online for updates and enhancements.

Investigation of Pt, Pt₃Co, and Pt₃Co/Mo Cathodes for the ORR in a Microfluidic H₂/O₂ Fuel Cell

Fikile R. Brushett,[a,*] Hung T. Duong,[b,*] Jia Wei "Desmond" Ng,[a,c] Rachel L. Behrens,[b,*] Andrzej Wieckowski,[b,**] and Paul J. A. Kenis[a,***,z]

[a]Department of Chemical and Biomolecular Engineering and [b]Department of Chemistry, University of Illinois at Urbana-Champaign, Urbana, Illinois 61801, USA

We report on the performance and durability of four Pt-based cathode catalysts in a microfluidic H₂/O₂ fuel cell: commercial unsupported Pt and Pt₃Co as well as in-house acid-treated Pt₃Co (Pt₃Co-at) and Pt₃Co/Mo. Commercial Pt₃Co was used as the starting material for both Pt₃Co-at and Pt₃Co/Mo. The composition of the resulting catalysts was confirmed via X-ray photoelectron spectroscopy analysis. In situ cathode studies were performed using an acidic microfluidic H₂/O₂ fuel cell with an analytical platform. The electrolyte flow rate was optimized to minimize the effects of water management such that fuel cell performance is kinetically limited by the oxygen reduction reaction (ORR). In addition, electrolyte concentration was separately varied to determine cathode performance as a function of acidic pH. All four catalysts demonstrated good short-term activity and stability under fuel cell operating conditions in harsh acidic environments, with the Pt₃Co/Mo alloy exhibiting the highest activity. Furthermore, both modified catalysts, Pt₃Co/Mo and Pt₃Co-at, exhibited superior durability compared to commercially available Pt₃Co and Pt in the accelerated cathode aging studies performed within the microfluidic fuel cell via potential cycling. In situ impedance analysis of the Pt₃Co/Mo cathode revealed enhanced catalyst stability and electrode durability as the cause of the dramatic improvements in long-term performance.
© 2010 The Electrochemical Society.   [DOI: 10.1149/1.3368721] All rights reserved.

For the widespread commercialization of small-scale fuel cell technologies, significant and simultaneous reductions in system costs (i.e., catalysts) and enhancements in activity and durability are required.[1-3] In particular, improving the cathodic oxygen reduction reaction (ORR) remains a key challenge. Sluggish kinetics and high overpotentials associated with the ORR hamper both energetic efficiency and peak power production.[4] Furthermore, the high cost and limited availability of platinum (Pt) necessitate the development of alternative catalysts, which either reduce or eliminate Pt content.[2] Many Pt-free oxygen reduction catalysts have been explored, including ruthenium-based chalcogenides,[5-7] metal oxides,[8] transition carbides,[9] cobalt–polypyrole–carbon composites,[10] enzymes,[11] and pyrolized porphyrins,[12-16] but none have shown the necessary combination of electrocatalytic activity and stability under acidic conditions to replace Pt-based catalysts in fuel cell systems. Alloying Pt with transition metals (i.e., M = Co, Ni, Fe, Cu, etc.) not only reduces catalyst costs by lowering Pt loading but can also increase the ORR activity over pure Pt in acidic media.[4,17-21] Recent work by Stamenkovic et al. suggests that Pt–Co alloys are the most promising of these Pt–M catalysts due to favorable shifts in Pt d-band energy centers, which alter the electronic structure and improve the ORR activity.[22] Several other factors have also been proposed as key contributors to the enhanced catalytic activity including, but not limited to, changes in the geometric structure (Pt–Pt bond distance), increased particle surface roughness, and particle size effects.[4,17,20-27] However, studies also indicate that under acidic conditions, the Pt–M alloys may exhibit instability and lose oxygen reduction activity due to leaching of the transition metals from the alloys.[2,28] According to Gasteiger et al., transition-metal dissolution is due to: (*i*) excess transition metal on the Pt surface, (*ii*) incomplete alloying of the two metals, and (*iii*) transition-metal leaching for a well-alloyed Pt–M catalyst under acidic fuel cell operating conditions.[2] Leaching of the transition metal from the catalyst surface cannot only reduce electrocatalytic activity, but also increase ohmic resistance and accelerate membrane electrode assembly degradation in polymer electrolyte membrane (PEM)-based fuel cells.[2,29-31] The surface dissolution of the transition metals can result

in a core-shell or a skeleton configuration that are comprised of Pt surface atoms with underlying transition-metal atoms.[21,24] The resulting geometric and electronic distortions lead to more stable enhancements of the ORR activity.[24,32] However, Antolini et al. observed that the reported stabilities of many Pt–M alloys in acidic environments are often conflicting and vary widely depending not only on experimental parameters (i.e., temperature, pressure, and pH) but also on material characteristics (i.e., degree of alloying) rather than just on the choice of a particular transition metal.[28] These findings demonstrate that the exact experimental configuration used for characterization can significantly impact reported Pt–M stabilities, as some reported results have observed high stabilities in the PEM-based fuel cells and low stabilities in half-cell setups for identical materials.[28]

Here, we compare the performance and durability of four different Pt-based cathode catalysts for the ORR in a previously developed microfluidic hydrogen–oxygen (H₂/O₂) fuel cell (Fig. 1), which functions as an analytical platform.[33,34] This configuration enables the experimental versatility of a traditional three-electrode electrochemical cell while operating as a true fuel cell. The four cathode catalysts investigated are commercial unsupported Pt and Pt₃Co, as well as in-house modified acid-treated Pt₃Co (samples referred to as Pt₃Co-at from here on) and Pt₃Co/Mo (Fig. 2). Others have shown that adding molybdenum (Mo) to palladium (Pd)-based oxygen reduction catalysts promotes activity, improves stability, and enhances carbon monoxide (CO) tolerance;[35,36] thus, the addition of Mo to an already ORR active catalyst, Pt₃Co, is investigated in this study. Ex situ character analyses of both catalyst materials before and after measurements, including the analysis of surface compositions, were confirmed via X-ray photoelectron spectroscopy (XPS) analysis.

Varying the parameters, such as flow rate, pH, and composition, of the aqueous electrolyte flowing between the two electrodes enables detailed performance analyses unencumbered by typical fuel cell limitations (i.e., water management and by-product removal). Moreover, in situ half-cell analyses of individual electrode characteristics can be compared over a wide range of fuel cell operating conditions (i.e., high current densities) by placing an external reference electrode at the electrolyte stream outlet.[33,57] These techniques were used to investigate the activity, stability, and durability of the four Pt-based catalysts as cathode materials over a range of experimental conditions through in situ chronoamperometric and impedance measurements in our microfluidic H₂/O₂ fuel cell.
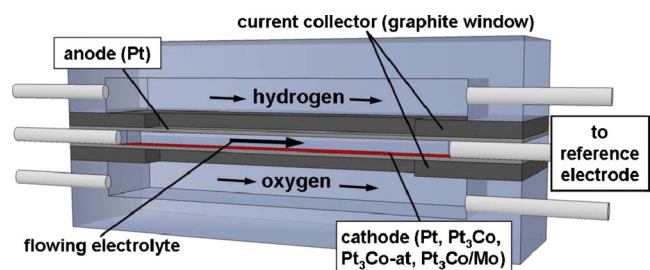
Figure 1. (Color online) Modular schematic of a microfluidic H_2/O_2 fuel cell that utilizes a flowing electrolyte stream and can serve as a catalyst/electrode characterization platform.

Experimental

Catalyst preparation.— All modification procedures started with 3–5 nm unsupported Pt_3Co (E-TEK) nanoparticles based upon manufacturer specification. To obtain the Pt_3Co/Mo nanoparticles, the mixture of as-received unsupported Pt_3Co nanoparticles, phosphomolybdic acid ($H_3PMo_{12}O_{40}$), and Millipore water was sonicated (3510 Branson) for 15 min before refluxing at 80°C under constant stirring and argon (Ar) flow for 1 h. After cooling the nanoparticle mixture to room temperature, 25 mL $NaBH_4/NaOH$ was added in a dropwise fashion under sonication. The solution was reheated to 80°C under constant stirring and Ar flow for 10 min and was then cooled to room temperature. The resulting Pt_3Co/Mo nanoparticles were filtered from the solution and rinsed with Millipore water (18.2 MΩ) to remove all unwanted residuals.

To obtain the acid pretreated nanoparticles, as-received Pt_3Co was loaded into a gold (Au) boat, which was carefully filled with 0.5 M H_2SO_4 so as not to dislodge the catalyst particles on the bottom of the boat. The catalyst was then cycled 40° times between 0 and 1.40 V vs reversible hydrogen electrode (RHE) at a scan rate of 50 mV/s.[32] After each modification, both the resulting catalysts, Pt_3Co/Mo and Pt_3Co-at, were filtered from the solution and rinsed with Millipore water (18.2 MΩ) to remove all unwanted residuals

XPS measurements.— XPS studies were performed on all Pt_3Co-based catalysts before and after modification procedures to confirm the changes in the surface structure and binding energies (BEs). A combined electrochemical and ultrahigh vacuum (UHV) XPS system was used so that electrochemical and XPS measurements could be conducted without sample exposure to the ambient environment during transfer between the electrochemical and UHV chambers.[32,38] For the XPS characterization, 5.0 mg/mL suspensions of desired catalyst nanoparticles in Millipore water were prepared.
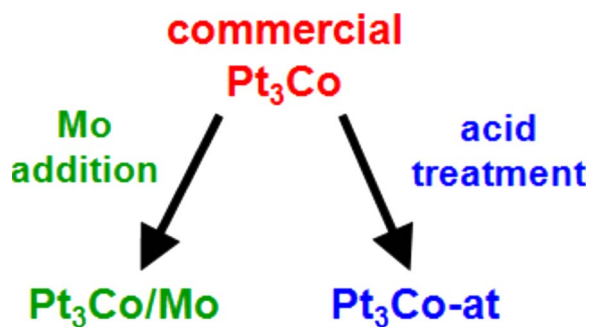
Figure 2. (Color online) Cartoon of cathode catalyst development strategy. The new catalyst materials of Pt_3Co/Mo and Pt_3Co-at were both modified from as-received, commercial unsupported Pt_3Co (Pt_3Co, E-TEK) via a Mo addition and a cyclic acid treatment, respectively. The activity and stability of all three catalysts (Pt_3Co, Pt_3Co-at, and Pt_3Co/Mo) were compared to Pt black (Pt, Alfa Aesar) over a range of experimental conditions.

After sonication for 30 min, 100 μL of catalyst suspension was deposited onto a gold disk, and the XPS measurements were taken. Using the M-Probe ESCA software, version 1.36 (Fisons Surface Science), the XPS spectral peaks were fitted using a mixed Gaussian–Lorentzian line shape and Shirley baselines. The BE scale was calibrated using Au $4f_{7/2}$ (at 84.0 eV) and Cu $2p_{3/2}$ (at 932.68 eV).[39]

CV measurements.— Cyclic voltammogram (CV) measurements were carried out using a three-electrode electrochemical cell with a rotating disk electrode (RDE, Autolab, EcoChemie) with a Au tip of 3 mm diameter (polished down to 3 μm), a Ag/AgCl ([Cl⁻] = 3 M, BAS) reference electrode (in a separate compartment), and a Pt wire (Alfa Aesar) counter electrode. Measurements were performed with a potentiostat (Autolab PGSTAT 100, EcoChemie). A 5.0 mg/mL suspension of the desired catalyst nanoparticles, either Pt black or Pt_3Co-based alloys, in Millipore water was prepared. After sonication for 30 min, 1 μL of the catalyst suspension was deposited on the RDE. The geometric surface area of the RDE was calculated to be 0.07 cm², and this value was used for the calculation of the current densities for the CVs. The CVs were measured in 0.5 M H_2SO_4 which was bubbled with nitrogen for 30 min before testing. For the Pt_3Co-based alloys, voltammograms were measured from 0 to 1.2 or 1.4 V vs RHE at a scan rate of 50 mV/s. For the comparative Pt black, the voltammogram was measured from 0 to 1.4 V vs RHE at a scan rate of 20 mV/s. The RDE was stationary for all measurements.

Gas diffusion electrode preparation.— Four different cathode catalysts were investigated: as-received Pt_3Co (Pt_3Co, E-TEK), Pt black (Pt, Alfa Aesar), (Pt_3Co-at), and Pt_3Co/Mo. For all studies, Pt black was used as the anode catalyst. Each catalyst ink was prepared by mixing 12 mg of the desired catalyst, 0.4 mg Nafion (5 wt % solution, Aldrich) as a binder, 200 μL Millipore water, and 200 μL isopropyl alcohol. The catalyst ink was sonicated (Branson 3510) for 2 h to obtain a uniform mixture, which was then painted on a Toray carbon paper gas diffusion layer (EFCG "S" type electrode, E-TEK) to create a gas diffusion electrode (GDE). The electrodes (geometric surface area: 4 cm²) were then hot-pressed (Carver 3851-0) at 340 psi (∼2344 kPa) and 120°C to ensure that the catalyst layer was compacted into the gas diffusion layer. All GDEs, both anode and cathode, had the 3 mg/cm² desired catalyst and 0.1 mg/cm² Nafion.

Fuel cell assembly and testing.— Two GDEs, anode and cathode, were placed on opposite sides of a 0.15 cm thick poly(methyl methacrylate) sheet, such that the catalyst-covered sides interfaced with the 3 cm long and 0.33 cm wide precision-machined window. The window had an inlet and an outlet on either side such that the aqueous sulfuric acid (H_2SO_4, GFS Chemicals, Inc., double distilled by Vycor) electrolyte flows between the electrodes. Two 0.1 cm thick graphite windows served as the current collectors. The hydrogen and oxygen gas flow chambers [5 cm (*L*) × 1 cm (*W*) × 0.5 cm (*H*)] were precision-machined into polycarbonate sheets. This multilayered assembly was held together using binder clips (Highmark). Fuel cell studies were conducted using a potentiostat (Autolab PGSTAT-30, EcoChemie) at room temperature with hydrogen and oxygen gas (laboratory grade, S.J. Smith), each at a flow rate of 50 sccm. Electrolyte flow rates were varied from 0.0 to 0.9 mL/min using a syringe pump (Harvard apparatus). The concentration of H_2SO_4 was varied from 0.25 to 3.0 M (approximate pH range of 0.6 to −0.48). Fuel cell polarization curves were obtained by steady-state chronoamperometric measurements at different cell potentials. All studies were conducted four times to ensure the immediate chemical and electrocatalytic stability of the cathodic materials under the acidic fuel cell operating conditions. Because all catalyst loadings were identical, 3 mg cat/cm², the exposed geometric electrode surface area (1 cm²) was used to calculate the current and power densities for the microfluidic H_2/O_2 fuel cell

tests. The aqueous electrolyte stream exited the fuel cell through a plastic tube (Cole Parmer, 1.57 mm i.d.) and was collected in a beaker. The polarization losses on the anode and the cathode were independently analyzed using multimeters (Fluke) by placing a Ag/AgCl reference electrode ($[Cl^-] = 3$ M, BAS) in the collection beaker.[33,34,37] No potential drop was observed along the plastic tubing connecting the fuel cell and the reference electrode.[37]

Electrochemical impedance spectroscopy (EIS) measurements were performed on the acidic microfluidic H_2/O_2 fuel cell operated with the five different cathode catalysts. AC impedance spectra were obtained using a frequency response analyzer module controlled by a potentiostat (Autolab PGSTAT-30, EcoChemie). The spectra were measured at a constant voltage mode by decreasing frequencies from 10 kHz to 30 mHz at 9 points/decade. The modulating voltage was 10 mV root-mean-squared. The measurements were performed at cell potentials ranging from 100 to 800 mV. The resulting Nyquist plots isolated the effects of the internal cell resistance (R_{cell}) and fuel cell electrode charge-transfer resistance (R_{ct}). Each measurement was performed three times.

Accelerated electrochemical aging.— By cycling electrodes across a potential range, catalyst dissolution rates were accelerated, leading to rapid performance losses due to a reduced electrochemical surface area. The rate and extent of these losses depended on the potential ranges and the cycle patterns (i.e., square waves vs cycles). Here, cathodes were aged in a three-electrode electrochemical cell via cyclic voltammetry under acidic conditions. Each cathode was cycled over a range of fuel cell operating potentials (0.10–1.00 V vs RHE) in 0.5 M H_2SO_4 for 1000-cycle sets at a 50 mV/s scan rate. After each set of 1000 cycles, the electrodes were rinsed with Millipore water to remove any residual acid. Between cycling sets, the cathodes were tested in an acidic microfluidic H_2/O_2 fuel cell to investigate the effects of aging on the electrode performance.

Results and Discussion

The activity, durability, and stability of the four catalysts, Pt, Pt_3Co, Pt_3Co-at, and Pt_3Co/Mo, were investigated as cathode materials under multiple experimental conditions using an acidic microfluidic H_2/O_2 fuel cell as an analytical platform. By varying the acidic electrolyte flow rate and concentration, we were able to compare the performances of the different cathodes at high current densities (at peak power density) within an operating fuel cell. Furthermore, accelerated aging studies by potential cycling offered insight into cathode durability under extended fuel cell operation. Ex situ analyses of the catalysts before and after measurements were performed by XPS and CV.

Ex situ characterization.— XPS studies were performed on the as-received Pt_3Co samples and the new samples, Pt_3Co-at and Pt_3Co/Mo, to characterize the surface chemical composition and to confirm the success of the modification procedures. The comparative XPS survey spectra of the commercial alloy before and after cyclic pretreatment under acidic conditions are shown in Fig. 3. For the commercial Pt_3Co sample, a nominal atomic Pt:Co ratio of 3:1 was determined from the XPS peak analysis (Fig. 3a), confirming the quality of the as-received sample. Cobalt (Co) peaks arise at 800 and 780 eV, corresponding to a Co $2p_{1/2}$ peak and a Co $2p_{3/2}$ peak, respectively.[32,40] The strong oxygen peak at 531 eV, along with the positive shift in the BE of the Co peaks, indicates a cobalt oxide surface species. Metallic Co is present as a shoulder in the Co $2p_{3/2}$ peak at 778 eV. Further quantitative analysis of the Co signals shows that $88 \pm 5\%$ is cobalt oxide and $12 \pm 5\%$ is metallic Co (Table I). After the acidic electrochemical pretreatment, the XPS spectrum shows a disappearance of the Co 2p and the O 1s peaks (Fig. 3b), but the platinum and the metallic Co peaks remain, which indicates that the surface cobalt oxides have dissolved.[32] This dissolution of the metal oxide species under acidic conditions causes a decrease in the oxygen reduction activity of the Pt–Co alloy.[2] However, the dissolution of the surface cobalt oxides from the nanoparticle sur-
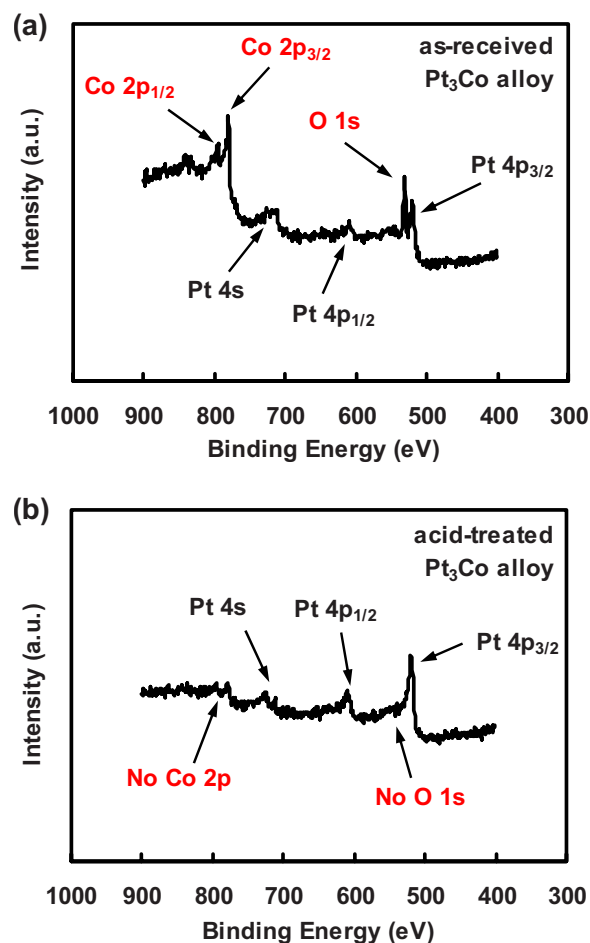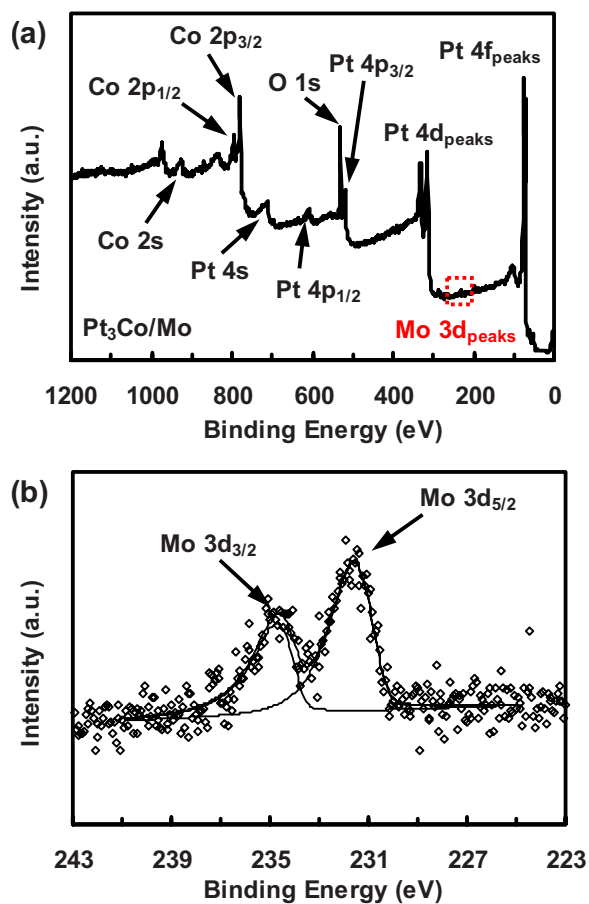

Figure 3. (Color online) XPS survey spectra of commercial Pt_3Co (E-TEK) (a) as-received and (b) after electrochemical pretreatment with key peaks labeled. The electrochemical pretreatment consisted of 40 cycles between 0 and 1.40 V vs RHE at 50 mV/s in 0.5 M H_2SO_4.

face leads to the formation of a core-shell catalyst particle or a skeleton structure with a Pt surface and a Co-rich layer beneath, enhancing the activity of the Pt–Co catalyst.[21,24] Here, the formation of a core-shell structure is further supported by the CV and XPS data. CVs of the as-received and pretreated Pt_3Co sample (Fig. 5a) show the removal of the Co surface species of the pretreated sample, as it now resembles the CV of pure Pt (Fig. 5b). Further XPS peak analysis of the acid pretreated Pt_3Co sample confirms the removal of all cobalt oxide species, yet Co is still present as metallic Co, beneath a protective Pt skin, which agrees with the CV (Fig. 5a), which lacks Co peaks; only those of Pt remain (Table I). More detailed XPS and electrochemical analyses of the Pt_3Co, Pt_3Co-at, and Pt catalysts may be found in a previous publication by Duong et al.[32]

The addition of Mo was added to the Pt_3Co catalysts to test the activity and stability, similar to the addition of Mo to Pd-based catalysts.[35,36] XPS survey spectra (Fig. 4) and CVs (Fig. 5c) were

Table I. Quantitative surface analysis of as-received Pt_3Co before and after electrochemical pretreatment in 0.5 M H_2SO_4.
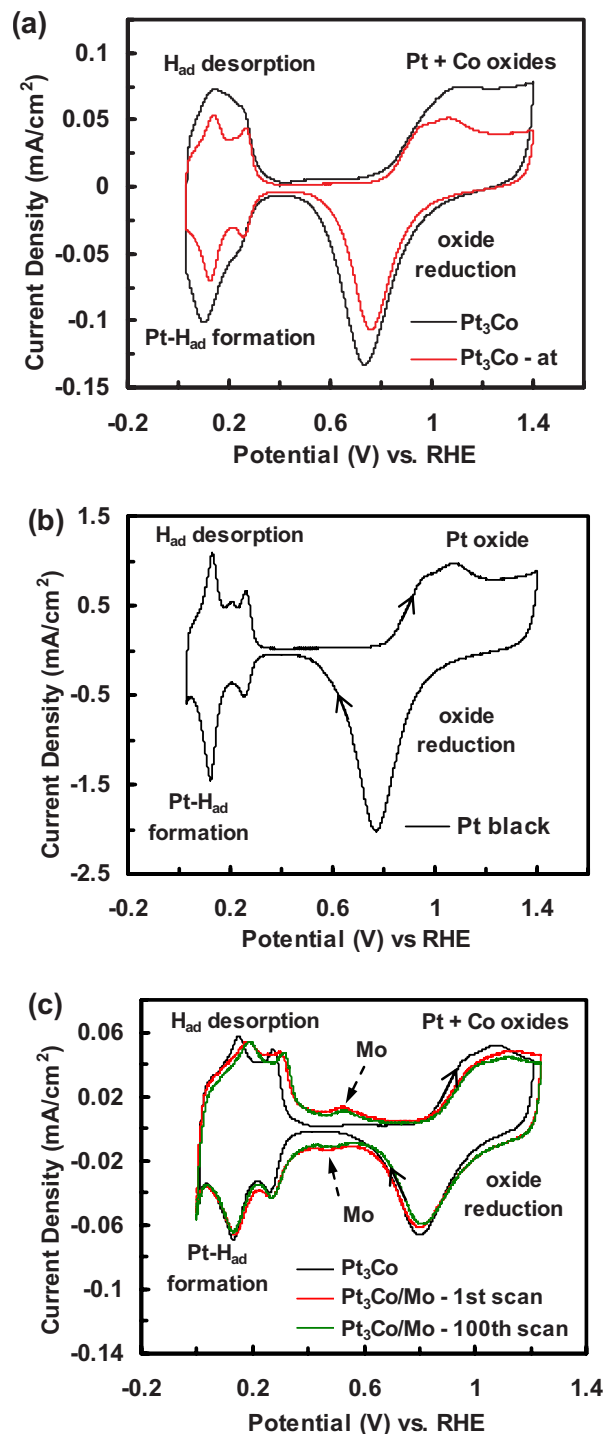
	Pt_3Co	Pt_3Co-at
Pt:Co ratio	3:1	36:1
Cobalt oxide concentration (%)	88 ± 5	0
Metallic cobalt concentration (%)	12 ± 5	100

Figure 4. (Color online) (a) XPS survey spectra of in-house modified Pt₃Co/Mo after the Mo modification. (b) Blown-up view of the 243–223 eV region. Box in part (a): The dual Mo peaks highlight the presence of Mo on the catalyst surface.

also performed to verify the successful molybdenum (Mo) deposition onto the Pt₃Co. Though difficult to discern from the broader survey spectra shown in Fig. 4a, small dual Mo peaks exist at 231 and 236 eV, confirming the deposition (Fig. 4b). Based upon the position of the BE peaks, Mo exists on the catalyst surface both in metallic form (Mo⁰ peak at 231 eV) and in oxide form (possibly Mo⁶⁺ peak at 236 eV).[40] From the peak analysis, nominal atomic ratios of 3:1 and 37:1 are determined for Pt:Co and Pt:Mo, respectively. Previous work by Raghuveer et al. and Sarkar et al. on the oxygen reduction activity of Pd–Co–Mo and Pd–Mo, respectively, demonstrated that catalytic performance decreased if alloys contain greater than 10 atom % Mo.[35,36] This decrease in the catalytic activity would be due to a reduction in electrochemically active surface sites, as the ORR does not occur on Mo. Therefore, a low deposition of the transition metal is favorable and is reflected in our Pt₃Co/Mo catalyst with a ∼2 to 3 atom % Mo.

The Mo addition to the Pt₃Co catalyst was also apparent in the CVs of Pt₃Co/Mo and Pt₃Co in 0.5 M H₂SO₄ (Fig. 5c). Distinctive oxidative and reductive peaks are observed around 0.5 V vs RHE on the Pt₃Co/Mo catalyst and indicate the presence of Mo species. This observation agrees well with the aforementioned XPS measurements and previously reported results.[41] Furthermore, the Pt₃Co/Mo catalyst immediately demonstrates improved stability compared to the as-received Pt₃Co catalyst under acidic conditions. Over 100 cycles, the Pt₃Co/Mo performance remains consistent with only marginal decreases in the Pt and Co oxide as well as Mo peaks, indicating minimal dissolution.


Figure 5. (Color online) CVs of Pt₃Co-based catalysts in 0.5 M H₂SO₄: (a) Commercial Pt₃Co and Pt₃Co-at and (c) commercial Pt₃Co and in-house modified Pt₃Co/Mo recorded at 50 mV/s. (b) For comparison, a CV of Pt black, recorded at 20 mV/s.

Effects of electrolyte flow rate.— The performance of an acidic microfluidic H₂/O₂ fuel cell operated with hot-pressed Pt electrodes, both anode and cathode, was investigated as a function of electrolyte flow rates (0.0, 0.3, 0.6, and 0.9 mL/min). Hydrogen and oxygen flow rates were 50 sccm each to ensure an adequate fuel and oxidant supply.[33] As shown in Fig. 6a and b, the polarization curves suggest that cell performance is limited by the cathode and is weakly dependent on the electrolyte flow rate. In prior work, we described in detail performance variations as a function of flow rate in this mi-

(a)

(b)

(c)
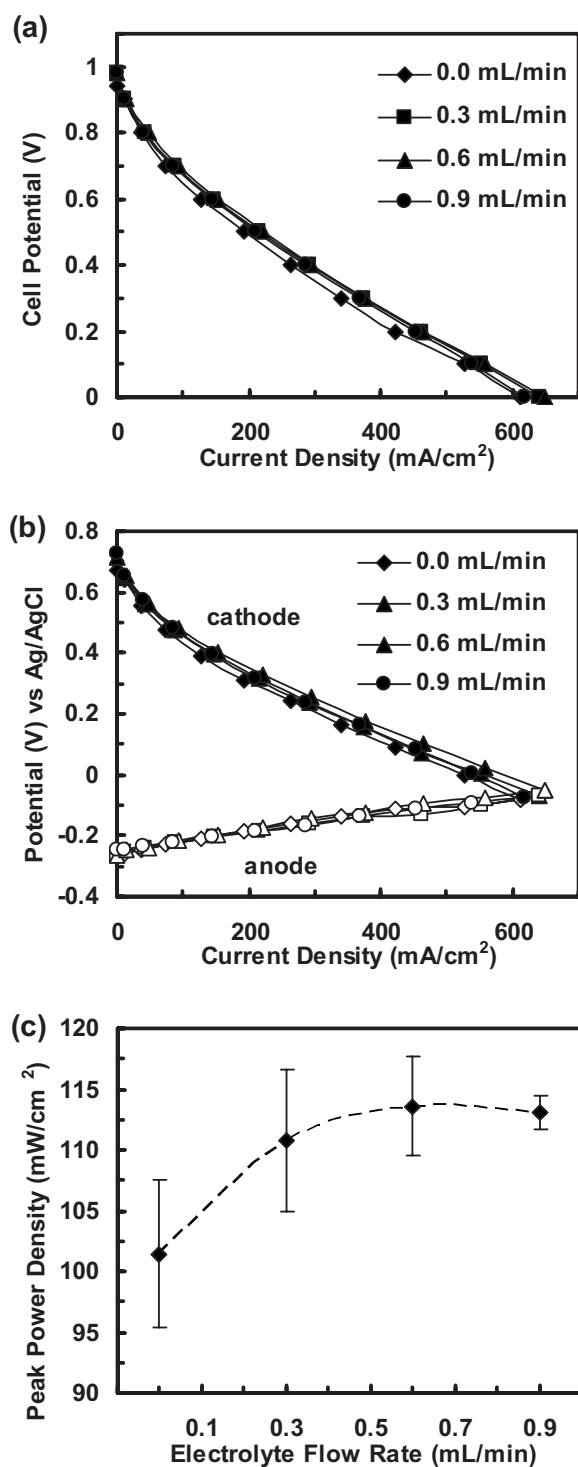
Figure 6. (a) Representative polarization curves for an acidic microfluidic H_2/O_2 fuel cell as a function of electrolyte flow rate (0.0, 0.3, 0.6, and 0.9 mL/min). (b) Corresponding representative anode and cathode polarization curves. (c) Peak power density of the fuel cell as a function of electrolyte flow rate ($N = 4$). Error bars represent a standard deviation from the average cell power density at each flow rate. In all studies, hydrogen and oxygen flow rates were 50 sccm each, electrode loadings were 3 mg Pt/cm², [H_2SO_4] was 0.5 M, and experiments were performed at room temperature.

crofluidic H_2/O_2 fuel cell, specifically with respect to water management at the cathode.[33] At high current densities, performance improvements are observed when utilizing a flowing electrolyte compared to a stationary electrolyte because the dynamic stream

(a)

(b)
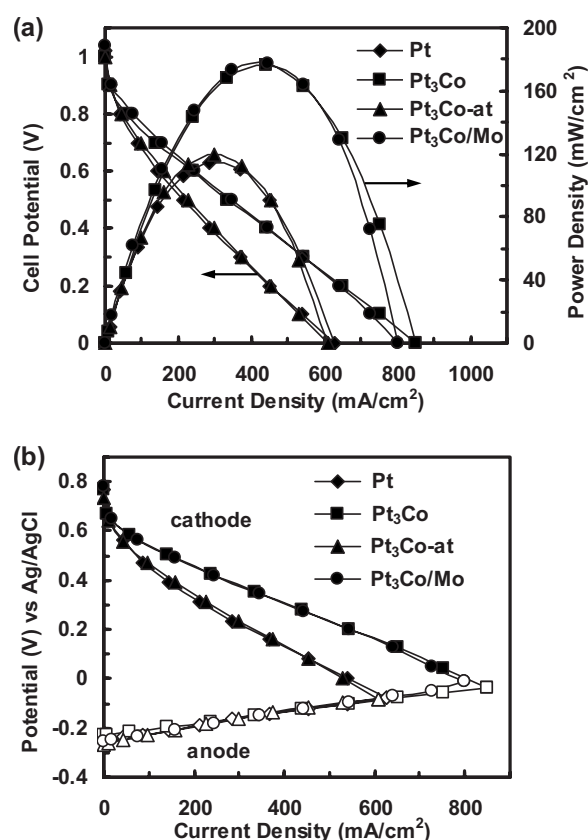
Figure 7. (a) Representative polarization and power density curves for an acidic microfluidic H_2/O_2 fuel cell as a function of cathode catalyst (Pt, Pt_3Co, Pt_3Co-at, and Pt_3Co/Mo). (b) Corresponding representative anode and cathode polarization curves. In all studies, a Pt black anode was used, and all electrode loadings were 3 mg cat/cm². Furthermore, hydrogen and oxygen flow rates were 50 sccm each, electrolyte flow rate was 0.6 mL/min, [H_2SO_4] was 0.5 M, and experiments were performed at room temperature.

facilitates water removal on the cathode. Individual electrode polarization curves confirm that any performance enhancements are due to improved water management at the cathode as the anode performance appears flow rate independent (Fig. 6b). Small enhancements are observed with increasing flow rate until 0.6 mL/min after which performance plateaus. At this point, the microfluidic configuration shifts from a mass-transfer limited regime, due to water removal from the cathode, to a kinetically limited regime, limited by ORR kinetics at the cathode. Cell peak power densities confirm an optimal electrolyte flow rate of 0.6 mL/min after which cell performance levels off (Fig. 6c). Furthermore, identical trends were observed with fuel cells operated with Pt_3Co and Pt_3Co/Mo cathodes, confirming that in the current configuration, ORR kinetics may be observed without significant interference from mass-transfer limitations at an electrolyte flow rate ≥0.6 mL/min. This flow rate dependence is also a function electrolyte concentration. Thus, while a flow rate of 0.6 mL/min is a transition point for 0.5 M H_2SO_4, this transition point flow rate would be reduced for lower concentrations and be elevated for higher concentrations. Also, the effects of hotpressing electrodes on transport processes within the GDE and consequent impact on the fuel cell performance are yet to be determined and will be addressed soon.

Cathode characterization.— Analyses of the four Pt-based cathodes were performed in a microfluidic H_2/O_2 fuel cell with a flowing acidic electrolyte of varying H_2SO_4 concentrations. Figure 7a shows comparative polarization and power density curves for the fuel cell operated with each cathode, and all cathodes demonstrated good oxygen reduction activity and chemical stability. Fuel cells

operated with either Pt_3Co or Pt_3Co/Mo cathodes exhibited enhanced performance over those with either Pt_3Co-at or Pt cathodes, and the performance shifts are due to changes in the oxygen reduction activity of the cathode catalysts (Fig. 7b). The core-shelled Pt_3Co-at cathode demonstrates slightly greater ORR activity than the Pt cathode, suggesting that the electrocatalytic properties of the core-shell nanoparticle are very similar to pure Pt despite the 25% reduction in Pt content. The Pt_3Co/Mo cathode exhibits slightly greater ORR activity than the Pt_3Co cathode and significantly greater ORR activity than the Pt cathode, suggesting that the Mo addition did not adversely affect catalytic activity.

Further in situ studies were performed at varying H_2SO_4 concentration from 0.25 to 3.0 M. The purpose of these studies is to analyze cathode performance and stability as a function of acid pH. The performance of the different cathodes is analyzed at peak power density ($V_{cell} = 0.4$ V) to simulate the high current densities typically observed in working fuel cells. As evident in Fig. 7b, the anode polarization curves are identical from experiment to experiment; thus, changes in cell performance may be attributed exclusively to different cathodes. Thus, while varying electrolyte concentration impacts the fuel cell flow rate dependence, comparative analyses may be performed on different cathode materials. Acidic microfluidic H_2/O_2 fuel cells operated with Pt_3Co or Pt_3Co/Mo cathodes significantly outperformed fuel cells operated with Pt or Pt_3Co-at over the range of H_2SO_4 concentrations (Fig. 8). Subtle effects on the fuel cell performance due to changes in acid concentration for Pt and Pt_3Co-at are shown in Fig. 8a, and those due to changes in acid concentration for Pt_3Co and Pt_3Co/Mo are shown in Fig. 8b. At H_2SO_4 concentrations ≤ 0.5 M, cell performance was limited by the increased cell resistance associated with the low electrolyte conductivity at these concentrations. At H_2SO_4 concentrations ≥ 2 M, cell performance leveled out and slightly decreased as increased sulfate/bisulfate poisoning reduced the active catalytic surface area available for reaction.[42,43] Furthermore, when operating the fuel cell with either Pt_3Co or Pt_3Co/Mo cathodes at high acid concentrations, when performance exceeds ~ 320 mW/cm^2, enough water was produced that the transport processes become insufficient and the cathode flooded. For milder acidic conditions (≤ 2 M), the Pt_3Co-at and Pt cathodes showed similar catalytic activities (Fig. 8a). At harsher conditions (≥ 2 M), the Pt cathode showed a slightly higher activity than the Pt_3Co-at cathode, which may be due to a greater number of active sites on the Pt cathode surface compared to the number of sites available on the Pt_3Co-at cathode surface. As shown in Fig, 8b, Pt_3Co/Mo cathodes slightly outperform Pt_3Co cathodes over the entire range of acidic conditions, suggesting that the Mo addition improves ORR activity. IR-correction analyses confirmed that all cathode performances were pH-independent for the pH range of 0.6 to −0.48 (0.25 to 3.0 M H_2SO_4).

Durability studies.— To test the long-term durability of the catalysts studied, accelerated cathode aging studies were performed in a three-electrode electrochemical cell where the electrodes were cycled multiple times over a range of fuel cell operating potentials, 0.1–1.00 V vs RHE, in 0.5 M H_2SO_4. Potential cycling is a widely used technique in fuel cell durability studies, both ex situ (i.e., RDE and GDE) and in situ (i.e., PEM-based fuel cells), as potential cycling under acidic conditions has been shown to expedite catalyst and electrode degradation.[3,29-31,44-52] First investigated by Kinoshita et al., potential cycling reduces the electrochemical active surface area of catalytic particles via metal dissolution into the acid and growth of larger particles at the expense of smaller particles, analogous to Ostwald ripening.[31,45] Reduced catalyst surface area decreases absolute activity and lowers fuel cell performance. The rate and extent of electrochemical surface area losses depend on potential ranges and on cycle patterns (i.e., square waves vs cycles). Previous studies have shown, at potentials greater than 0.8 V vs RHE, increased dissolution rates, and, consequently, reduced catalyst and fuel cell performances are observed for the Pt and Pt–M alloy catalysts in both in situ and ex situ studies.[31,47-52]
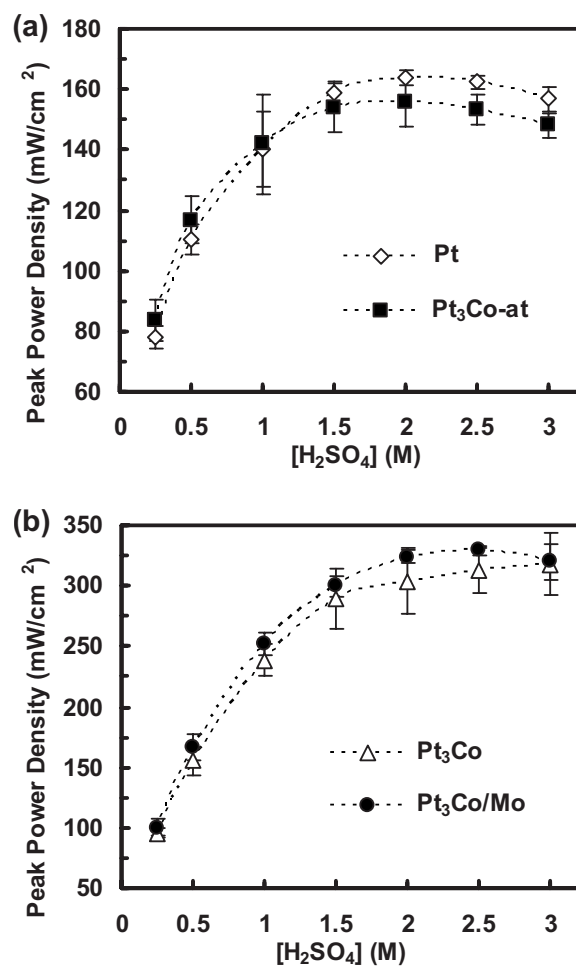
Figure 8. Peak power densities of microfluidic H_2/O_2 fuel cell operated with different cathodes, (a) Pt and Pt_3Co-at and (b) Pt_3Co and Pt_3Co/Mo, as a function of flowing [H_2SO_4] ($N = 4$). Error bars represent a standard deviation from the average cell power density at each [H_2SO_4]. In all studies, a Pt anode was used, and all electrode loadings were 3 mg cat/cm^2. Furthermore, hydrogen and oxygen flow rates were 50 sccm each, electrolyte flow rate was 0.6 mL/min, and experiments were performed at room temperature.

After each 1000-cycle set, cathode performance was investigated in an acidic microfluidic H_2/O_2 fuel cell. Peak power densities for the fuel cell operated with each cathode studied as a function of cathode aging are shown in Fig. 9a. Over the course of the 10,000 cathode aging cycle, the peak performance of Pt, Pt_3Co, Pt_3Co-at, and Pt_3Co/Mo decreased by 11.8, 33.2, 1.9, and 8.3%, respectively (Table II). Both modified cathode catalysts, Pt_3Co-at and Pt_3Co/Mo, demonstrated superior durability, compared to Pt and Pt_3Co, in acidic environments under fuel cell operating potentials. Over the course of 10,000 cycles, the performance of the as-received Pt_3Co activity reduces to that of the Pt_3Co-at, which seems to indicate a complete loss of cobalt oxide species from the catalytic surface of the core-shelled particle. Despite a modest overall improvement in catalytic performance, the enhanced stability and reduced Pt content make the core-shelled Pt_3Co a viable alternative to pure Pt as a fuel cell cathode catalyst.

The dramatically enhanced durability of the Pt_3Co/Mo cathode compared to that of the Pt_3Co cathode is a very promising result. By performing EIS measurements on the acidic microfluidic H_2/O_2 fuel operated with fresh (0 cycles) or aged (10,000 cycles) Pt_3Co and Pt_3Co/Mo cathodes, the root causes of the improved durability may be determined. Figure 9b and c shows the representative Nyquist plots of the fuel cell studies conducted with fresh and aged Pt_3Co
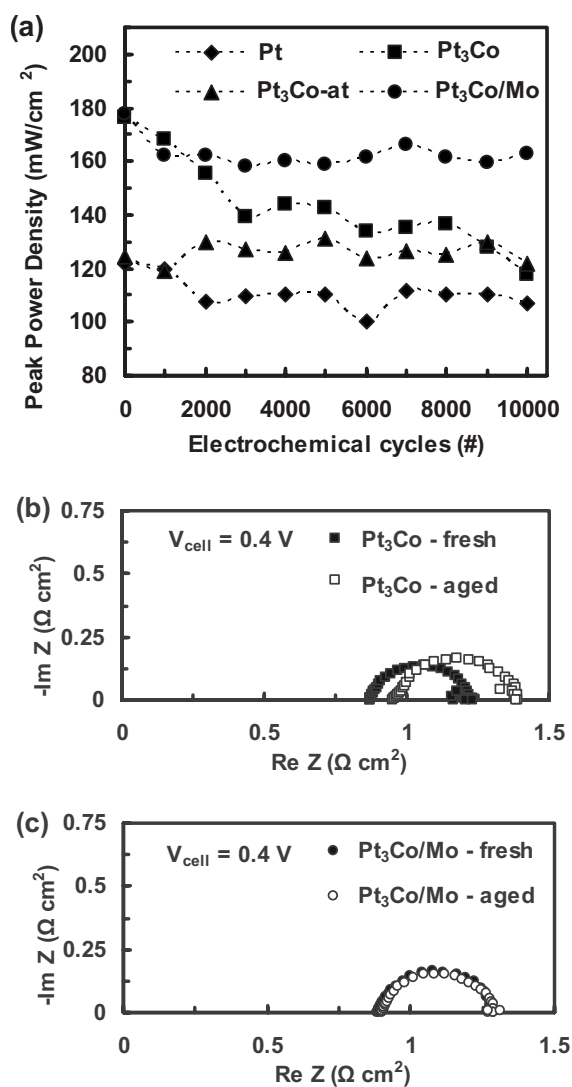
Figure 9. (a) Peak power densities of acidic microfluidic H_2/O_2 fuel cell operated with different cathodes (Pt, Pt_3Co, Pt_3Co-at, and Pt_3Co/Mo) as a function of electrochemical cathode aging, specifically potential sweep cycles. Nyquist plots of fuel cell performance with fresh (0 cycles) and aged (10,000 cycles) when using (b) a Pt_3Co cathode or (c) a Pt_3Co/Mo cathode. For fuel cell studies, a Pt anode was used and all electrode loadings were 3 mg cat/cm^2. Furthermore, hydrogen and oxygen flow rates were 50 sccm each, electrolyte flow rate was 0.6 mL/min, [H_2SO_4] was 0.5 M, and experiments were performed at room temperature.

Table III. Cell resistance (R_{cell}), charge-transfer resistance (R_{ct}), and total resistance (R_{tot}) for microfluidic fuel cells operated with fresh (0 cycles) and aged (10,000 cycles) Pt_3Co and Pt_3Co/Mo cathodes ($N = 3$). In all studies, hydrogen and oxygen flow rates were 50 sccm each, electrolyte flow rate was 0.6 mL/min, [H_2SO_4] was 0.5 M, and experiments were performed at room temperature. For all studies, a fresh Pt black anode was used.

Cathode catalyst		R_{cell} (Ω cm^2)	R_{ct} (Ω cm^2)	R_{tot} (Ω cm^2)
Pt_3Co	Fresh	0.875 ± 0.008	0.284 ± 0.052	1.159 ± 0.053
	Aged	0.992 ± 0.099	0.399 ± 0.033	1.391 ± 0.104
	Difference	0.117 ± 0.099	0.115 ± 0.062	0.232 ± 0.117
Pt_3Co/Mo	Fresh	0.912 ± 0.034	0.357 ± 0.059	1.269 ± 0.068
	Aged	0.949 ± 0.056	0.386 ± 0.030	1.335 ± 0.064
	Difference	0.038 ± 0.065	0.029 ± 0.066	0.067 ± 0.093

and Pt_3Co/Mo cathodes, respectively, at a cell potential of 0.4 V, the potential at which peak power densities were observed. For all experiments, the same fresh Pt anode was used; thus, comparative shifts in the impedance spectra can be attributed to the changes in the different cathode materials. The high frequency intercept on the *x*-axis (initial data point closest to the origin in Fig. 9b and c) represents the cell resistance (R_{cell}), which includes electrolyte solution resistance and any ohmic resistances in the fuel cell components (i.e., catalyst layer, gas diffusion layer, and current collectors).[53] As the experimental setup and operating conditions are identical, the differences between the measured cell resistances and the calculated electrolyte solution resistance (0.635 Ω cm^2 in 0.5 M H_2SO_4)[54] can be attributed to the changes in cathode internal resistance, which varies as a function of electrochemical aging and the catalyst used. In general, as the R_{cell} increases due to greater electrode resistances, the electrode and overall fuel cell performance decrease. An increase in R_{cell}, as a function of aging, is observed for fuel cells operated with the Pt_3Co cathode (Fig. 9b). No increase in R_{cell} is observed for fuel cells operated with the Pt_3Co/Mo cathode (Fig. 9c). This increase in R_{cell} may be attributed to Co leaching from the unsupported Pt_3Co nanoparticles under acidic fuel cell operating conditions, adversely affecting adhesion between the catalyst and gas diffusion layers, which increases contact resistances. These qualitative observations suggest that the Mo addition to the Pt_3Co nanoparticles prevents leaching of Co species.

The two fuel cell electrode reactions, represented by the semicircular features in each Nyquist plot, can be described by two parallel R_{ct}-C_{cpe} circuits with different time constants. Here, C_{cpe} is a constant phase element capacitance describing the porous, distributed nature of the GDEs and R_{ct} is the overall fuel cell charge-transfer resistance represented by the diameter of the semicircle. In acidic media, hydrogen oxidation reaction kinetics are rapid and contribute minimally to the overall R_{ct} response.[55] Thus, the sluggish cathodic ORR kinetics are the dominant contribution to the measured R_{ct}. An increase in R_{ct}, as a function of aging, is observed for fuel cells operated with the Pt_3Co cathode (Fig. 9b). No increase in R_{cell} is observed for the fuel cells operated with the Pt_3Co/Mo (Fig. 9c). This increase in R_{ct} can again be attributed to Co leaching for the unsupported Pt_3Co nanoparticles, which reduces the ORR activity, thus lowering the cathode and overall fuel cell performance. These qualitative observations suggest that the Pt_3Co/Mo retains a high ORR activity, despite electrochemical aging, by minimizing Co leaching from the Pt alloy.

To quantitatively analyze the trends shown in the representative Nyquist plots in Fig. 9b and c, all experiments were performed in triplicate to account for any cell-to-cell variations resulting from (*i*) differences in assembly/disassembly and (*ii*) differences in exact operating parameters due to the nature of the syringe pump used to drive the electrolyte flow. The critical R_{cell} and R_{ct} values as well as the total resistance (R_{tot}), as shown in Table III, for fuel cells oper-

Table II. Peak power density losses in an acidic microfluidic H_2/O_2 fuel cell as a function of cathode aging before and after 10,000 cycles. Accelerated aging studies performed in a three-electrode electrochemical cell in 0.5 M H_2SO_4 cycling between 0.10 and 1.00 V vs RHE at a 50 mV/s scan rate. For all studies, a fresh Pt black anode was used.

Cathode catalyst	Peak power density (mW/cm^2)		Decrease (%)
	0 cycles	10,000 cycles	
Pt	121.6	107.2	11.8
Pt_3Co	176.0	117.6	33.2
Pt_3Co-at	124.4	122.0	1.9
Pt_3Co/Mo	177.6	162.8	8.3

ated with fresh and aged Pt_3Co and Pt_3Co/Mo cathodes. With the Pt_3Co as the cathode, the measured R_{cell} increased from 0.875 ± 0.008 to 0.992 ± 0.099 Ω cm^2 as a function of electrochemical aging. This corresponds to an increase in 0.117 ± 0.099 Ω cm^2 in the R_{cell}. In contrast, when using Pt_3Co/Mo cathodes, the measured R_{cell} increased from 0.912 ± 0.034 to 0.949 ± 0.056 Ω cm^2 due to aging. This negligible increase in 0.038 ± 0.065 Ω cm^2 in the R_{cell} confirms that the Pt_3Co/Mo cathode structure does not degrade significantly over the course of the electrochemical aging.

Furthermore, while operating the fuel cell with Pt_3Co cathodes, the measured R_{ct} increased from 0.284 ± 0.052 to 0.399 ± 0.033 Ω cm^2 as a function of aging (Table III). This corresponds to an increase in 0.115 ± 0.062 Ω cm^2 in the R_{ct}. In contrast, when using the Pt_3Co/Mo cathodes, the measured R_{ct} changed from 0.357 ± 0.059 to 0.386 ± 0.030 Ω cm^2 as a function of aging. This negligible increase in 0.029 ± 0.066 Ω cm^2 in the R_{ct} confirms that the Pt_3Co/Mo cathode activity does not reduce significantly over the course of the electrochemical aging. The quantitative observations suggest that Pt_3Co/Mo cathodes outperform Pt_3Co cathodes by minimizing transition-metal leaching for the catalyst surface. Also, the effects of Co leaching are twofold: (*i*) an increase in the internal electrode resistance and (*ii*) a decrease in the ORR activity. Consequently, the improved performance observed for the Pt_3Co/Mo cathodes may be attributed to the dual effects of enhanced electrode and catalyst stability, but further work would be needed to confirm this.

Conclusions

Lack of low cost cathode catalysts with suitable activity and durability remains a key obstacle that hinders the widespread commercialization of fuel cell technologies. Pt–M alloys demonstrate enhanced oxygen reduction activity compared to Pt, but these alloys often exhibit insufficient stability under acidic fuel cell operating conditions. Here, the performance and durability of several Pt-based cathode catalysts were probed in a microfluidic H_2/O_2 fuel cell with a flowing acidic electrolyte. An excellent catalyst/electrode characterization tool, this analytical platform enables detailed in situ investigations of the performance of individual components over a range of experimental conditions that are traditionally limited to a three-electrode electrochemical cell. Core-shell Pt_3Co (Pt_3Co-at) and Mo-modified Pt_3Co (Pt_3Co/Mo) catalysts were modified from a commercially available Pt_3Co catalyst. The XPS measurements confirmed the successful modification of the catalyst surface composition for the catalysts studied.

In situ cathode studies were performed in an acidic fuel cell to determine the oxygen reduction activity and stability of the three Pt_3Co-based alloys, and their performance was compared to unsupported Pt, the current cathode catalyst of choice. The electrode analysis of hot-pressed GDE performance indicated that the dynamic electrolyte stream improved water removal at the cathode surface, but at flow rates ≥ 0.6 mL/min fuel cell performance became kinetically limited by the ORR for the operation at 0.5 M H_2SO_4. All the cathode catalysts (Pt, Pt_3Co, Pt_3Co-at, and Pt_3Co/Mo) studied exhibited good short-term chemical stability and electroactivity in an operating fuel cell at varying acid concentrations. Due to largely similar surface compositions, Pt_3Co-at and Pt cathode performances were comparable. Under milder acidic conditions, the Pt_3Co-at cathode slightly outperformed the Pt cathode, while under harsher conditions, the Pt cathode performance was superior. These observations may be due to the differences in the structure of the respective nanoparticle surfaces, such as the variation in the activity and in the number of catalytic sites. The Pt_3Co/Mo cathode outperformed the Pt_3Co cathode over the range of pH, indicating that the modification of Pt_3Co with Mo indeed resulted in an improved ORR activity.

In accelerated durability studies, both the modified cathode catalysts, Pt_3Co-at and Pt_3Co/Mo, demonstrate improved long-term sta-

bility compared to both Pt and Pt_3Co. The Pt_3Co-at cathode demonstrates a superior long-term stability, compared to all the other catalysts. Thus, despite modest overall performance improvements, various core-shell Pt_3Co cathode catalysts represent a viable alternative to the commonly used Pt due to their reduced Pt content (lower costs) and enhanced durability. The dramatically enhanced durability of the Pt_3Co catalyst with the Mo addition was further investigated via impedance analysis to reveal the source as dual improvements in catalytic stability and electrode durability.

While the development of core-shell Pt–M alloys is an area of intense ongoing investigation, to our knowledge Pt–Co–Mo alloys have not been used as ORR catalysts previously. Building on these promising results and drawing from reported Pd–Co–Mo and Pd–Mo alloy studies,[35,36] further development and optimization of catalyst modification procedures, e.g., through tailoring of Pt:M ratios, may lead to marked enhancement in oxygen reduction activity. Furthermore, adding capabilities to the microfluidic electrochemical platform would benefit catalyst/electrode performance and durability studies. For example, the integration of an in situ analyses of effluent electrolyte compositions facilitates a study of catalyst degradation patterns.

References

1. M. Jacoby, *Chem. Eng. News*, **87**, 39 (2009).
2. H. A. Gasteiger, S. S. Kocha, B. Sompalli, and F. T. Wagner, *Appl. Catal., B*, **56**, 9 (2005).
3. R. Borup, J. Meyers, B. Pivovar, Y. S. Kim, R. Mukundan, N. Garland, D. Myers, M. Wilson, F. Garzon, D. Wood, et al., *Chem. Rev. (Washington, D.C.)*, **107**, 3904 (2007).
4. J. K. Nørskov, J. Rossmeisl, A. Logadottir, L. Lindqvist, J. R. Kitchin, T. Bligaard, and H. Jonsson, *J. Phys. Chem. B*, **108**, 17886 (2004).
5. D. X. Cao, A. Wieckowski, J. Inukai, and N. Alonso-Vante, *J. Electrochem. Soc.*, **153**, A869 (2006).
6. D. T. Whipple, R. S. Jayashree, D. Egas, N. Alonso-Vante, and P. J. A. Kenis, *Electrochim. Acta*, **54**, 4384 (2009).
7. N. A. Vante and H. Tributsch, *Nature (London)*, **323**, 431 (1986).
8. L. Jorissen, *J. Power Sources*, **155**, 23 (2006).
9. H. Meng and P. K. Shen, *Electrochem. Commun.*, **8**, 588 (2006).
10. R. Bashyam and P. Zelenay, *Nature (London)*, **443**, 63 (2006).
11. J. A. Cracknell, K. A. Vincent, and F. A. Armstrong, *Chem. Rev. (Washington, D.C.)*, **108**, 2439 (2008).
12. M. Lefevre, E. Proietti, F. Jaouen, and J. P. Dodelet, *Science*, **324**, 71 (2009).
13. H. A. Gasteiger and N. M. Markovic, *Science*, **324**, 48 (2009).
14. J. Fournier, G. Lalande, R. Cote, D. Guay, and J. P. Dodelet, *J. Electrochem. Soc.*, **144**, 218 (1997).
15. S. L. Gojkovic, S. Gupta, and R. F. Savinell, *J. Electroanal. Chem.*, **462**, 63 (1999).
16. F. Jaouen and J. P. Dodelet, *Electrochim. Acta*, **52**, 5975 (2007).
17. T. Toda, H. Igarashi, H. Uchida, and M. Watanabe, *J. Electrochem. Soc.*, **146**, 3750 (1999).
18. P. Mani, R. Srivastava, and P. Strasser, *J. Phys. Chem. C*, **112**, 2770 (2008).
19. V. R. Stamenkovic, B. Fowler, B. S. Mun, G. F. Wang, P. N. Ross, C. A. Lucas, and N. M. Markovic, *Science*, **315**, 493 (2007).
20. S. Mukerjee and S. Srinivasan, *J. Electroanal. Chem.*, **357**, 201 (1993).
21. S. Chen, P. J. Ferreira, W. C. Sheng, N. Yabuuchi, L. F. Allard, and Y. Shao-Horn, *J. Am. Chem. Soc.*, **130**, 13818 (2008).
22. V. Stamenkovic, B. S. Mun, K. J. J. Mayrhofer, P. N. Ross, N. M. Markovic, J. Rossmeisl, J. Greeley, and J. K. Norskov, *Angew. Chem., Int. Ed.*, **45**, 2897 (2006).
23. V. Stamenkovic, T. J. Schmidt, P. N. Ross, and N. M. Markovic, *J. Electroanal. Chem.*, **554–555**, 191 (2003).
24. V. R. Stamenkovic, B. S. Mun, K. J. J. Mayrhofer, P. N. Ross, and N. M. Markovic, *J. Am. Chem. Soc.*, **128**, 8813 (2006).
25. M. Watanabe, K. Tsurumi, T. Mizukami, T. Nakamura, and P. Stonehart, *J. Electrochem. Soc.*, **141**, 2659 (1994).

26. B. C. Beard and P. N. Ross, *J. Electrochem. Soc.*, **137**, 3368 (1990).
27. K. Yamamoto, T. Imaoka, W. J. Chun, E. Osamu, H. Katoh, M. Takenaga, and A. Sonoi, *Nat. Chem.*, **1**, 397 (2009).
28. E. Antolini, J. R. C. Salgado, and E. R. Gonzalez, *J. Power Sources*, **160**, 957 (2006).
29. J. Aragane, T. Murahashi, and T. Odaka, *J. Electrochem. Soc.*, **135**, 844 (1988).
30. K. Yasuda, A. Taniguchi, T. Akita, T. Ioroi, and Z. Siroma, *Phys. Chem. Chem. Phys.*, **8**, 746 (2006).
31. Y. Shao-Horn, W. C. Sheng, S. Chen, P. J. Ferreira, E. F. Holby, and D. Morgan, *Top. Catal.*, **46**, 285 (2007).
32. H. T. Duong, M. A. Rigsby, W. P. Zhou, and A. Wieckowski, *J. Phys. Chem. C*, **111**, 13460 (2007).
33. R. S. Jayashree, M. Mitchell, D. Natarajan, L. J. Markoski, and P. J. A. Kenis, *Langmuir*, **23**, 6871 (2007).
34. F. R. Brushett, W. P. Zhou, R. S. Jayashree, and P. J. A. Kenis, *J. Electrochem. Soc.*, **156**, B565 (2009).
35. V. Raghuveer, A. Manthiram, and A. J. Bard, *J. Phys. Chem. B*, **109**, 22909 (2005).
36. A. Sarkar, A. V. Murugan, and A. Manthiram, *J. Phys. Chem. C*, **112**, 12037 (2008).
37. E. R. Choban, P. Waszczuk, and P. J. A. Kenis, *Electrochem. Solid-State Lett.*, **8**, A348 (2005).
38. C. Vericat, M. Wakisaka, R. Haasch, P. S. Bagus, and A. Wieckowski, *J. Solid State Electrochem.*, **8**, 794 (2004).
39. M. P. Seah, L. S. Gilmore, and G. Beamson, *Surf. Interface Anal.*, **26**, 642 (1998).
40. C. D. Wagner, A. V. Naumkin, A. Kraut-Vass, J. W. Allison, C. J. Powell, and J. R. Rumble, Jr., http://srdata.nist.gov/xps/, date last accessed 2009.
41. D. dos Anjos, K. Kokoh, J. M. Léger, A. R. Andrade, P. Olivi, and G. Tremiliosi-Filho, *J. Appl. Electrochem.*, **36**, 1391 (2006).
42. G. Horanyi, in *Interfacial Electrochemistry: Theory, Experiment, and Application*, A. Wieckowski, Editor, p. 477, Marcel Dekker, New York (1999).
43. M. E. Gamboa-Aldeco, E. Herrero, P. S. Zelenay, and A. Wieckowski, *J. Electroanal. Chem.*, **348**, 451 (1993).
44. C. H. Paik, G. S. Saloka, and G. W. Graham, *Electrochem. Solid-State Lett.*, **10**, B39 (2007).
45. K. Kinoshita, J. T. Lundquist, and P. Stonehart, *J. Electroanal. Chem. Interfacial Electrochem.*, **48**, 157 (1973).
46. B. Merzougui and S. Swathirajan, *J. Electrochem. Soc.*, **153**, A2220 (2006).
47. H. R. Colón-Mercado, H. Kim, and B. N. Popov, *Electrochem. Commun.*, **6**, 795 (2004).
48. H. R. Colón-Mercado and B. N. Popov, *J. Power Sources*, **155**, 253 (2006).
49. S. C. Zignani, E. Antolini, and E. R. Gonzalez, *J. Power Sources*, **182**, 83 (2008).
50. Y. Y. Shao, G. P. Yin, and Y. Z. Gao, *J. Power Sources*, **171**, 558 (2007).
51. P. Yu, M. Pemberton, and P. Plasse, *J. Power Sources*, **144**, 11 (2005).
52. X. W. Yu and S. Y. Ye, *J. Power Sources*, **172**, 145 (2007).
53. M. Ciureanu and R. Roberge, *J. Phys. Chem. B*, **105**, 3531 (2001).
54. G. Prentice, *Electrochemical Engineering Principles*, Prentice-Hall, Englewood Cliffs, NJ (1991).
55. S. Srinivasan, *Fuel Cells: From Fundamentals to Applications*, Springer, New York (2006).